

## SHAPING THE DUST MASS – STAR-FORMATION RATE RELATION

JENS HJORTH<sup>1</sup>, CHRISTA GALL<sup>1,2,3</sup>, AND MICHAŁ J. MICHAŁOWSKI<sup>4,5,6</sup>

Received 2013 November 25; accepted 2014 January 21

### ABSTRACT

There is a remarkably tight relation between the observationally inferred dust masses and star-formation rates (SFRs) of SDSS galaxies,  $M_{\text{dust}} \propto \text{SFR}^{1.11}$  (da Cunha et al. 2010). Here we extend the  $M_{\text{dust}}$ –SFR relation to the high end and show that it bends over at very large SFRs (i.e., dust masses are lower than predicted for a given SFR). We identify several distinct evolutionary processes in the diagram: (1) A *star-bursting phase* in which dust builds up rapidly at early times. The maximum attainable dust mass in this process is the cause of the bend-over of the relation. A high dust-formation efficiency, a bottom-light initial mass function, and negligible supernova shock dust destruction are required to produce sufficiently high dust masses. (2) A *quiescent star-forming phase* in which the subsequent parallel decline in dust mass and SFR gives rise to the  $M_{\text{dust}}$ –SFR relation, through astration and dust destruction. The dust-to-gas ratio is approximately constant along the relation. We show that the power-law slope of the  $M_{\text{dust}}$ –SFR relation is inversely proportional to the global Schmidt–Kennicutt law exponent (i.e.,  $\sim 0.9$ ) in simple chemical evolution models. (3) A *quenching phase* which causes star formation to drop while the dust mass stays roughly constant or drops proportionally. Combined with *merging*, these processes, as well as the range in total baryonic mass, give rise to a complex population of the diagram which adds significant scatter to the original  $M_{\text{dust}}$ –SFR relation. (4) At very high redshifts, a population of galaxies located significantly below the local relation is predicted.

*Subject headings:* dust, extinction — galaxies: evolution — galaxies: high-redshift — galaxies: ISM

### 1. INTRODUCTION

Galactic scaling relations such as the ‘main sequence of star formation’ (the relation between star-formation rate and stellar mass, see Noeske et al. 2007; Daddi et al. 2007; Wuyts et al. 2011) provide important constraints on galaxy evolution models and the physical processes involved.

One such relation reflects that massive star-forming galaxies contain large amounts of dust while old elliptical (red and dead) galaxies do not. This qualitative notion was quantified by da Cunha et al. (2010) who showed that for SDSS galaxies there is a tight  $M_{\text{dust}}$ –SFR relation,  $M_{\text{dust}} \sim \text{SFR}^{1.11 \pm 0.01}$ . The  $M_{\text{dust}}$ –SFR relation presented by da Cunha et al. (2010) consists of 3258 low-redshift SDSS galaxies with complementary data from GALEX, 2MASS and IRAS. The 1653 data points with the highest signal-to-noise ratio are reproduced in Figure 1 (blue data points).

Naively, one might interpret this to be a causal relation, either due to star formation induced by the prior presence of dust as seeds for star formation (although this poses the question of where the initial amounts of dust come from in the first place) or as a direct consequence

of dust produced following massive star formation (or, rather, death). However, da Cunha et al. (2010) advocated a different scenario in which the relation emerges as a consequence of the parallel decline of dust and SFR due to the decreasing gas mass available for star formation as time goes on and a simultaneous decline in total dust mass due to dust destruction.

To shed further light on the  $M_{\text{dust}}$ –SFR relation we here populate the da Cunha et al. (2010) observational diagram with additional classes of galaxies. In particular, in Section 2 we extend it to higher SFR and  $M_{\text{dust}}$  by including sub-millimeter galaxies (SMGs). These galaxies bring important new insight into the physical origin of the relation. In Section 3 we model the extended relation using simple chemical evolution models for massive galaxies, both from a simple analytical perspective and using full numerical models. In particular, we show that the slope of the relation can be related to the exponent of the Schmidt–Kennicutt star-formation law, relating the SFR to the available gas reservoir. Finally, in Section 4, we discuss how starbursts, quiescent star formation and quenching of the star formation cause galaxies to move around in the diagram and contribute to the significant scatter revealed here.

### 2. THE $M_{\text{dust}}$ –SFR RELATION

We supplement the original da Cunha et al. (2010)  $M_{\text{dust}}$ –SFR relation with the *Herschel* early-type galaxies (ETGs) and passive spirals studied by Rowlands et al. (2012). These are plotted in Figure 1 as red filled (ETGs) and open (spirals) circles. The Milky Way data point is taken from Hjorth et al. (2014). For SMGs we use recent ALMA based data points from Swinbank et al. (2013).

The da Cunha et al. (2010) and Rowlands et al. (2012) data points are for a Chabrier (2003) initial mass func-

<sup>1</sup> Dark Cosmology Centre, Niels Bohr Institute, University of Copenhagen, Juliane Maries Vej 30, DK-2100 Copenhagen Ø, Denmark

<sup>2</sup> Department of Physics and Astronomy, Aarhus University, Ny Munkegade 120, DK-8000 Aarhus C, Denmark

<sup>3</sup> NASA, Goddard Space Flight Center, 8800 Greenbelt Road, Greenbelt, MD 20771

<sup>4</sup> Sterrenkundig Observatorium, Universiteit Gent, Krijgslaan 281-S9, 9000, Gent, Belgium

<sup>5</sup> SUPA (Scottish Universities Physics Alliance), Institute for Astronomy, University of Edinburgh, Royal Observatory, Edinburgh, EH9 3HJ, UK

<sup>6</sup> FWO Pegasus Marie Curie Fellow

tion (IMF) and a dust mass absorption coefficient of  $0.77 \text{ cm}^2 \text{ g}^{-1}$  at  $850 \mu\text{m}$ , as implemented in MAGPHYS (da Cunha et al. 2008). The Swinbank et al. (2013) SFR was obtained by multiplying the far-infrared luminosity by  $10^{-10} M_{\odot} L_{\odot}^{-1} \text{ yr}^{-1}$  (appropriate for a Chabrier IMF; the UV contribution to the total SFR in SMGs is negligible). The quoted dust masses were multiplied by  $1.5/0.77$  to rescale to the same dust mass absorption coefficient. We note that while the literature data have been scaled to the same IMF and dust mass absorption coefficient, systematic offsets in the different subsamples may remain, due to different wavelength coverage, redshift, and methods of analysis used. For example, the lack of long-wavelength ( $> 100 \mu\text{m}$ ) data in da Cunha et al. (2010) may bias dust temperatures high and hence dust masses low (Smith et al. 2012).

The da Cunha et al. (2010) relation (shown as a thick pale-blue dashed line) does not extend to very high SFRs and dust masses. Extrapolating the relation to high SFRs shows that observed dust masses are about an order of magnitude smaller than predicted (this effect would be even stronger if the da Cunha et al. (2010) dust masses are underestimated). It is also evident that the relation is not as sharply defined as suggested by the SDSS galaxies alone. We discuss these effects below.

### 3. EVOLUTION OF DUST AND STAR FORMATION IN MASSIVE GALAXIES

Chemical evolution models can be used to study the temporal evolution of dust, gas, abundance distribution of elements, stellar mass and metallicity in a galaxy. The models are governed by processes regulating the evolution of a galaxy and, thus, are useful to study not only the chemical history but also to trace the SFR and the effects of the IMF, gas flows, and dust destruction and growth processes. Chemical evolution models have been applied to diverse types of galaxies, such as the Milky Way (see Dwek 1998; Calura et al. 2008; Zhukovska et al. 2008, and references therein), high-redshift galaxies (e.g., Edmunds 2001; Morgan & Edmunds 2003) or high- $z$  quasars (e.g., Dwek et al. 2007; Gall et al. 2011b).

#### 3.1. Basic equations

In this Letter we model a galaxy as a homogeneous entity (no spatial dependence of its properties) and with no infalling or outflowing material (closed box approximation). Efficient supernova (SN) dust production is assumed, while dust grain growth in the interstellar medium (ISM) is not explicitly considered. Relevant rates are assumed to be independent of metallicity. The model is described in detail in Gall et al. (2011a), whose notation we adopt.

The rate of change of the total dust mass is

$$\frac{dM_{\text{d}}}{dt} = E_{\text{d,SN}}(t) + E_{\text{d,AGB}}(t) - E_{\text{D}}(t), \quad (1)$$

where  $E_{\text{d,SN}}(t)$  and  $E_{\text{d,AGB}}(t)$  are the dust injection rates of SNe and asymptotic giant branch (AGB) stars, respectively. The SN dust production rate is

$$E_{\text{d,SN}}(t) = \int_{m_{\text{L}}}^{m_{\text{U}}} Y_{\text{Z}}(m) \epsilon_{\text{SN}}(m) \psi(t - \tau(m)) \phi(m) dm, \quad (2)$$

where  $m_{\text{L}}$  and  $m_{\text{U}}$  are the lower and upper mass limits for stars exploding as SNe,  $Y_{\text{Z}}(m)$  is the mass of ejected metal yields per SN,  $\epsilon_{\text{SN}}(m)$  is the SN dust production efficiency as defined in Gall et al. (2011c),  $\psi(t)$  is the SFR,  $\tau(m)$  is the main sequence lifetime of a star with mass  $m$ , and  $\phi(m)$  is the IMF, normalized in the interval  $[m_1, m_2]$  as  $\int_{m_1}^{m_2} m \phi(m) dm = 1$ , with  $m_1$  and  $m_2$  being the low and high mass cutoffs for the adopted IMF, respectively. The rate of dust destruction due to astration and shocks in the interstellar medium (e.g., McKee 1989; Jones et al. 1996), respectively, is defined as

$$E_{\text{D}}(t) = \eta_{\text{d}}(t) \psi(t) + M_{\text{cl}} R_{\text{SN}}(t), \quad (3)$$

where  $M_{\text{cl}}$  is the mass of interstellar material swept up and cleared of dust by a single SN, and

$$R_{\text{SN}}(t) = \int_{m_{\text{L}}}^{m_{\text{U}}} \psi(t - \tau) \phi(m) dm \quad (4)$$

is the SN rate. The dust-to-ISM ratio is

$$\eta_{\text{d}}(t) = \frac{M_{\text{d}}(t)}{M_{\text{ISM}}(t)}, \quad (5)$$

where

$$M_{\text{ISM}}(t) = M_{\text{d}}(t) + M_{\text{g}}(t). \quad (6)$$

The equation for the evolution of the gas mass is

$$\frac{dM_{\text{g}}}{dt} = E_{\text{g}}(t) + \eta_{\text{d}}(t) M_{\text{cl}} R_{\text{SN}}(t) - \psi(t) (1 - \eta_{\text{d}}(t)), \quad (7)$$

where  $E_{\text{g}}(t)$  is the rate of gaseous material returned to the ISM.

Finally, we assume a global star-formation law, inspired by the Schmidt–Kennicutt law (Schmidt 1959; Kennicutt 1998),

$$\psi(t) = \psi_{\text{ini}} \left( \frac{M_{\text{ISM}}(t)}{M_{\text{ini}}} \right)^k, \quad (8)$$

(Equation (2) in Gall et al. 2011a), where  $\psi_{\text{ini}}$  and  $M_{\text{ini}}$  are the initial SFR and gas mass, and  $k$  is the global Schmidt–Kennicutt exponent, usually taken to be 1.0 or 1.5 (Dwek et al. 2007; Calura et al. 2008).

#### 3.2. Approximations and simplifications

We next introduce several simplifications which will allow us to capture the essentials (but not the details) of the chemical evolution equations:

We assume that SN yields are released into the ISM instantly after the progenitor star is born, i.e.,  $\tau \approx 0$ , in which case

$$R_{\text{SN}}(t) = \gamma \psi(t), \quad (9)$$

where

$$\gamma = \int_{m_{\text{L}}}^{m_{\text{U}}} \phi(m) dm \quad (10)$$

is the SN rate to SFR ratio.

We ignore the contribution from AGB stars (e.g., Dwek et al. 2007; Michałowski et al. 2010a; Gall et al. 2011c) or other sources to the evolution of the dust mass, so

$$\frac{dM_{\text{d}}}{dt} = E_{\text{d,SN}}(t) - E_{\text{D}}(t), \quad (11)$$

with

$$E_{d,\text{SN}}(t) = \mu_D \psi(t) \quad (12)$$

and

$$E_D(t) = \beta \eta_d(t) \psi(t), \quad (13)$$

where  $\mu_D$  is the dust productivity (Gall et al. 2011c), and

$$\beta = 1 + \gamma M_{\text{cl}}. \quad (14)$$

The resulting equation for the evolution of the dust mass is

$$\frac{dM_d}{dt} = (\mu_D - \beta \eta_d(t)) \psi(t). \quad (15)$$

We also assume that  $\eta_d \ll 1$  (e.g., Tielens 2005; Gall et al. 2011a) and that  $E_g(t) \propto \psi(t)$ , so the evolution of gas mass is

$$\frac{dM_g}{dt} = -\delta \psi(t), \quad (16)$$

where  $\delta$  is a constant of proportionality close to unity, and

$$\psi(t) = \alpha M_g(t)^k; \quad \alpha = \frac{\psi_{\text{ini}}}{M_{\text{ini}}^k}. \quad (17)$$

We study IMFs with  $\phi(m) \propto m^{-2.35} \exp(-m_{\text{ch}}/m)$  with  $m_L = 8 M_\odot$  and  $m_U = 40 M_\odot$ ,  $m_1 = 0.1 M_\odot$  and  $m_2 = 100 M_\odot$ , and maximum SN dust production efficiency (Gall et al. 2011c), corresponding to an average dust yield per SN of  $\sim 0.3\text{--}0.4 M_\odot$  (Hjorth et al. 2014). In particular, we study Salpeter ( $m_{\text{ch}} = 0$ ) and bottom-light ( $m_{\text{ch}} = 10 M_\odot$ ) IMFs for which the conversions to Chabrier IMF SFRs are 1/1.8 and 3.0 (see, for example, Dwek et al. 2011). For a bottom-light (Salpeter) IMF, the approximate values of the parameters entering are  $\gamma \approx 0.02$  ( $0.007$ )  $M_\odot^{-1}$ ,  $\delta \approx 0.83$ ,  $\mu_D \approx 0.018$  ( $0.003$ ),  $M_{\text{cl}} = 0\text{--}1500 M_\odot$ , and  $\beta = 1\text{--}30$ .

### 3.3. Analytical results

We next investigate simple analytical limiting cases at early and late times resulting from the above set of equations.

#### 3.3.1. Early times: The starburst limit

At early times, not much gas has been consumed, so  $M_g \approx M_{\text{ini}}$  and  $\psi \approx \psi_{\text{ini}}$ . Thus

$$\frac{dM_d}{dt} = \mu_D \psi_{\text{ini}} - \frac{\beta \psi_{\text{ini}}}{M_{\text{ini}}} M_d(t) \quad (18)$$

and so

$$M_d(t) = \frac{\mu_D}{\beta} M_{\text{ini}} \left( 1 - \exp\left(-\beta \frac{\psi_{\text{ini}}}{M_{\text{ini}}} t\right) \right). \quad (19)$$

In other words the maximum attainable dust mass is  $M_d(t)/M_{\text{ini}} = \mu_D/\beta$  and for  $\beta t \ll \beta t_0 \equiv M_{\text{ini}}/\psi_{\text{ini}}$ ,  $M_d(t) = \mu_D \psi_{\text{ini}} t$  (see also Gall et al. 2011c), i.e.,  $M_d(t_0) = 0.63(\mu_D/\beta) M_{\text{ini}}$ . For a bottom-light IMF ( $\mu_D = 0.018$ ), SNe will turn of order 1% of the initial total mass into dust in the absence of dust destruction ( $\beta = 1$ ), independent of the initial SFR.

During this early phase, the dust mass is proportional to the SFR and the duration of the starburst. However, this is not the  $M_{\text{dust}}\text{--SFR}$  relation we are seeking. To reach the dust levels observed, the galaxies

would have been forming dust at a steady level for  $t = M_d(t)/(\mu_D \psi_{\text{ini}}) \approx 4$  Gyr (for a Salpeter IMF). While in some cases such an interpretation may be viable (e.g., for the Milky Way, see Hjorth et al. 2014), in general this time scale is uncomfortably long and the scenario is not expected to give rise to such a well-defined relation.

#### 3.3.2. Late times: quiescent star formation and the slope of the $M_{\text{dust}}\text{--SFR}$ relation

At late times, star formation will decrease because of the reduced availability of gas. As a consequence of the lower SN rate, there is less dust production. The dust destruction term is a combination of consumption through astration and grain destruction due to SN shocks.

We seek a relation consistent with the  $M_{\text{dust}}\text{--SFR}$  relation and therefore make the *ansatz*

$$M_d = A \psi^B. \quad (20)$$

From this follows that

$$\frac{dM_d}{dt} = -ABk\delta\alpha^{1/k}\psi^{B+1-1/k}. \quad (21)$$

Requiring the exponent of  $\psi$  in Equations (15) and (21) to be equal, i.e.,  $1 = B + 1 - 1/k$ , yields  $B = 1/k$ . In other words,

$$M_d = A \psi^{1/k} \quad (22)$$

and hence  $M_d \propto M_g$ , i.e., a constant dust-to-gas ratio,  $\eta_d$ , during the late, non-starbursting phase. Indeed, requiring the prefactors of Equations (15) and (21) to be equal,  $\mu_D - \eta_d(t)\beta = -ABk\delta\alpha^{1/k}$ , shows that  $\eta_d(t)$  must be time independent. The net dust evolution term is negative and equals  $-A\delta\alpha^{1/k}$ .

Note that for  $k = 1.5$ ,  $M_d \propto \psi^{2/3}$ , while for  $k = 0.9$  one retrieves the da Cunha et al. (2010)  $M_{\text{dust}}\text{--SFR}$  relation,  $M_d \propto \psi^{1.11}$ .

### 3.4. Numerical models

For illustration we compute full chemical evolution models with an initial mass of  $M_{\text{ini}} = 3 \times 10^{11} M_\odot$ , initial SFRs corresponding to a Chabrier SFR of  $\psi_{\text{ini}} = 1000 M_\odot \text{ yr}^{-1}$ , a range of SN dust destruction clearing masses ( $M_{\text{cl}} = 0\text{--}1500 M_\odot$ ), and for Salpeter or bottom-light IMFs (for details see Gall et al. 2011a).

Regarding the Schmidt–Kennicutt slope (exponent denoted by  $N$  for surface densities,  $\Sigma_{\text{SFR}} \propto \Sigma_{\text{mol}}^N$ ), Kennicutt (1998) found a slope of  $1.4 \pm 0.15$  (for a recent review, see Kennicutt & Evans 2012). Krumholz et al. (2012) argue on theoretical grounds that the local volumetric relation between SFR and gas should be  $\rho_{\text{SFR}} \propto \rho_{\text{gas}}^{1.5}$ . The models of Renaud et al. (2012) however suggest the slope is closer to unity at high densities or SFRs, due to stellar feedback. Indeed, Freundlich et al. (2013) find  $N \approx 1$  in resolved galaxies at  $z \approx 1.2$  while Leroy et al. (2013) find  $N = 1 \pm 0.15$  for the relation between molecular mass and SFR in nearby galaxies. Shetty et al. (2014) find a non-universal slope whose average is  $N = 0.76 \pm 0.16(2\sigma)$ . Calura et al. (2008) use  $k = 1$  in their models of proto E galaxies. We here compute models with  $k$  ranging from 0.9 to 1.2 and evolve them over 10 Gyr.

We plot the models in Figure 1. As a benchmark model (thick solid curve) we choose a bottom-light IMF,

no SN dust destruction, and  $k = 0.9$  to match the observed  $M_{\text{dust}}$ -SFR relation. The dashed curve shows the corresponding Salpeter IMF model, while the dotted curves show the effect of varying the SN dust destruction clearing mass,  $M_{\text{cl}}$ , for a bottom-light IMF. These models confirm that the power-law slope of the  $M_{\text{dust}}$ -SFR relation at late times is consistent with  $1/k$ . The differing IMFs or clearing masses primarily affect the normalization of the curves. The IMF has a strong effect on the total amount of dust produced, with bottom-light IMFs leading to significantly (up to an order of magnitude) higher dust masses, for a fixed (Chabrier IMF equivalent) SFR, confirming previous findings (Dwek et al. 2007; Michałowski et al. 2010b; Gall et al. 2011a,b,c; Valiante et al. 2011; Dwek et al. 2011). More massive systems (not shown) also lead to higher dust masses. Thin solid lines show the effect of varying  $k$  and confirms the expected  $1/k$  behavior. We verified that incorporation of AGB stars does not change the overall qualitative behaviour of the models presented here.

#### 4. DISCUSSION

As shown by da Cunha et al. (2010), using Calura et al. (2008) chemical evolution models, the  $M_{\text{dust}}$ -SFR relation can be interpreted as an evolutionary sequence. This is partly confirmed by our analysis. In this picture, the initial phase is due to a starburst in which dust is built up at essentially constant star formation rate. Due to the maximum attainable dust mass derived in Section 3.3.1, the SMG data points are located, on average, below the extrapolation of the linear fit to the SDSS data points (da Cunha et al. 2010). We note that to reproduce the highest dust masses, very efficient formation of dust from the metals produced by SNe is required (see also Michałowski et al. 2010b; Gall et al. 2011b). The Calura et al. (2008) models do not reproduce such high dust masses. The high end of the  $M_{\text{dust}}$ -SFR relation is therefore further evidence for a surprisingly efficient and rapid dust formation process at work, such as that inferred from SN 1987A (Matsuura et al. 2011; Indebetouw et al. 2014). Presumably the dust is either formed directly in SNe or through rapid subsequent grain growth in the ejecta/remnant or the ISM, such that the majority of the refractory elements available are turned into dust. We note that, for the highest dust masses, significant SN dust destruction is not allowed by the models.

The numerical models also confirm that the late evolution is characterized by a joint decay in dust mass and SFR rate which leads to a power-law relation between them, with a slope of  $1/k$ . Hence, the slope of the  $M_{\text{dust}}$ -SFR relation can be directly related to the global incarnation (Equation 8) of the Schmidt-Kennicutt star-formation law (Schmidt 1959; Kennicutt 1998). We note that the commonly adopted value of  $k = 1.5$  is not favored by the models which seem to prefer values around  $1 \pm 0.2$ . The joint decay in these quantities is due to a delicate balance between continued star and dust formation and the parallel consumption of the available gas (and dust) reservoir and through dust destruction by SN shocks. The balance is characterized by a roughly constant dust-to-gas ratio along the  $M_{\text{dust}}$ -SFR relation.

We may consider the early and late phases to be two

stages of star formation; the first being the rapid starburst when all the dust is formed, the second being quiescently star-forming galaxies. Of course, the “initial” starburst in the chemical evolution model need not necessarily refer to the very beginning of the evolution of a galaxy – it may for example relate to the time when a lot of gas ( $M_{\text{ini}}$ ) is supplied to the galaxy (e.g., through a merger). It is also possible that some galaxies undergo several starbursts. Other processes may be at work in shaping the  $M_{\text{dust}}$ -SFR diagram. Quenching of star formation will lead to a rapid decline in the SFR. If this is due to removal of cold gas and dust from the galaxy (e.g., due to heating or expulsion, Hopkins et al. 2008), a parallel decline in the dust mass will lead to a transition more or less parallel to the  $M_{\text{dust}}$ -SFR relation. However, if the star formation is quenched but the dust retained (e.g., when the cold gas reservoir, such as a gaseous galactic disk, becomes stable against fragmentation to bound clumps, so-called morphological quenching, see Martig et al. 2009; Genzel et al. 2013) then a horizontal transition is expected. Conversely, merging will produce a parallel upwards evolution along the  $M_{\text{dust}}$ -SFR relation, perhaps leading to a subsequent starburst.

We stress that the evolutionary models plotted in Figure 1 are for illustration and are not intended to account for all the data points being part of a single evolutionary sequence. Notably, the *Herschel* ETGs and passive spirals (red symbols) appear, on average, to be offset from the relation (blue points), with higher dust masses at a given SFR, or, equivalently, lower SFR at a given dust mass. Part of the effect may be due to their average higher masses, a selection effect in that they are *Herschel* detected, or morphological quenching as discussed above. Long-time sustained low star formation from a large gas reservoir appears unlikely to account for the full effect given they are early-type galaxies. It is interesting to note that the offsets of the *Herschel* ETGs and the SMGs from the main relation are reminiscent of the similar offsets of such galaxies from the main sequence of star formation, i.e., the  $M_*$ -SFR relation. Possibly, the SMGs and the *Herschel* ETGs form a separate evolutionary sequence, characterized by a higher  $k$ .

As suggested by the models, we expect a population of star-bursting galaxies significantly below the relation. Because of the logarithmic scale and the short amount of time spent in this early phase, such galaxies may be rare. Examples include the low-metallicity low-redshift dwarf galaxy starbursts I Zw 18 (Fisher et al. 2013) and SBS 0035–052 (Hunt et al. 2014). At higher redshifts, entering the era of reionization, we expect most galaxies to have low dust content because of the limited time available since Big Bang and the onset of star formation. ALMA should uncover a significant population of very high redshift galaxies below the local relation. The  $z \sim 6.6$  galaxy ‘Himiko’ may be one such candidate (Ouchi et al. 2013).

Given the heterogeneous data sets used, as well as the possible range of model parameters (initial mass, SFR, and IMF in particular) and evolutionary processes entering, one expects quite some scatter in the relation, as revealed here. More homogeneous samples would be needed to model evolutionary sequences in more detail.

We thank Haley Gomez, Julie Wardlow, Sune Toft, Stefano Zibetti, Anna Gallazzi, and Darach Watson for discussions, and Elisabete da Cunha and Mark Swinbank for making their data points available in electronic form. The anonymous referee provided very insightful comments. C.G. was supported from the NASA Postdoctoral Program (NPP) and acknowledges funding provided by the Danish Agency for Science and Technology and Innovation. The Dark Cosmology Centre is funded by the Danish National Research Foundation.

## REFERENCES

- Calura, F., Pipino, A., & Matteucci, F. 2008, *A&A*, 479, 669  
 Chabrier, G. 2003, *PASP*, 115, 763  
 da Cunha, E., Charlot, S., & Elbaz, D. 2008, *MNRAS*, 388, 1595  
 da Cunha, E., Eminian, C., Charlot, S., & Blaizot, J. 2010, *MNRAS*, 403, 1894  
 Daddi, E., et al. 2007, *ApJ*, 670, 156  
 Dwek, E. 1998, *ApJ*, 501, 643  
 Dwek, E., Galliano, F., & Jones, A. P. 2007, *ApJ*, 662, 927  
 Dwek, E., et al. 2011, *ApJ*, 738, 36  
 Edmunds, M. G. 2001, *MNRAS*, 328, 223  
 Fisher, D. B., et al. 2013, arXiv:1310.4842  
 Freundlich, J., et al. 2013, *A&A*, 553, A130  
 Gall, C., Andersen, A. C., & Hjorth, J. 2011a, *A&A*, 528, A13  
 —. 2011b, *A&A*, 528, A14  
 Gall, C., Hjorth, J., & Andersen, A. C. 2011c, *A&A Rev.*, 19, 43  
 Genzel, R., et al. 2013, arXiv:1310.3838  
 Hjorth, J., et al. 2014, in preparation  
 Hopkins, P. F., Hernquist, L., Cox, T. J., & Kereš, D. 2008, *ApJS*, 175, 356  
 Hunt, L. K., et al. 2014, *A&A*, 561, A49  
 Indebetouw, R., et al. 2014, *ApJ*, 782, L2  
 Jones, A. P., Tielens, A. G. G. M., & Hollenbach, D. J. 1996, *ApJ*, 469, 740  
 Kennicutt, R. C., & Evans, N. J. 2012, *ARA&A*, 50, 531  
 Kennicutt, Jr., R. C. 1998, *ApJ*, 498, 541  
 Krumholz, M. R., Dekel, A., & McKee, C. F. 2012, *ApJ*, 745, 69  
 Leroy, A. K., et al. 2013, *AJ*, 146, 19  
 Martig, M., Bournaud, F., Teyssier, R., & Dekel, A. 2009, *ApJ*, 707, 250  
 Matsuura, M., et al. 2011, *Science*, 333, 1258  
 McKee, C. 1989, in *IAU Symposium*, Vol. 135, *Interstellar Dust*, ed. L. J. Allamandola & A. G. G. M. Tielens, 431  
 Michałowski, M. J., Murphy, E. J., Hjorth, J., Watson, D., Gall, C., & Dunlop, J. S. 2010a, *A&A*, 522, A15  
 Michałowski, M. J., Watson, D., & Hjorth, J. 2010b, *ApJ*, 712, 942  
 Morgan, H. L., & Edmunds, M. G. 2003, *MNRAS*, 343, 427  
 Noeske, K. G., et al. 2007, *ApJ*, 660, L43  
 Ouchi, M., et al. 2013, *ApJ*, 778, 102  
 Renaud, F., Kraljic, K., & Bournaud, F. 2012, *ApJ*, 760, L16  
 Rowlands, K., et al. 2012, *MNRAS*, 419, 2545  
 Schmidt, M. 1959, *ApJ*, 129, 243  
 Shetty, R., Kelly, B. C., Rahman, N., Bigiel, F., Bolatto, A. D., Clark, P. C., Klessen, R. S., & Konstantin, L. K. 2014, *MNRAS*, 437, L61  
 Smith, D. J. B., et al. 2012, *MNRAS*, 427, 703  
 Swinbank, M., et al. 2013, arXiv:1310.6362  
 Tielens, A. G. G. M. 2005, *The Physics and Chemistry of the Interstellar Medium*  
 Valiante, R., Schneider, R., Salvadori, S., & Bianchi, S. 2011, *MNRAS*, 416, 1916  
 Wuyts, S., et al. 2011, *ApJ*, 742, 96  
 Zhukovska, S., Gail, H.-P., & Tieloff, M. 2008, *A&A*, 479, 453

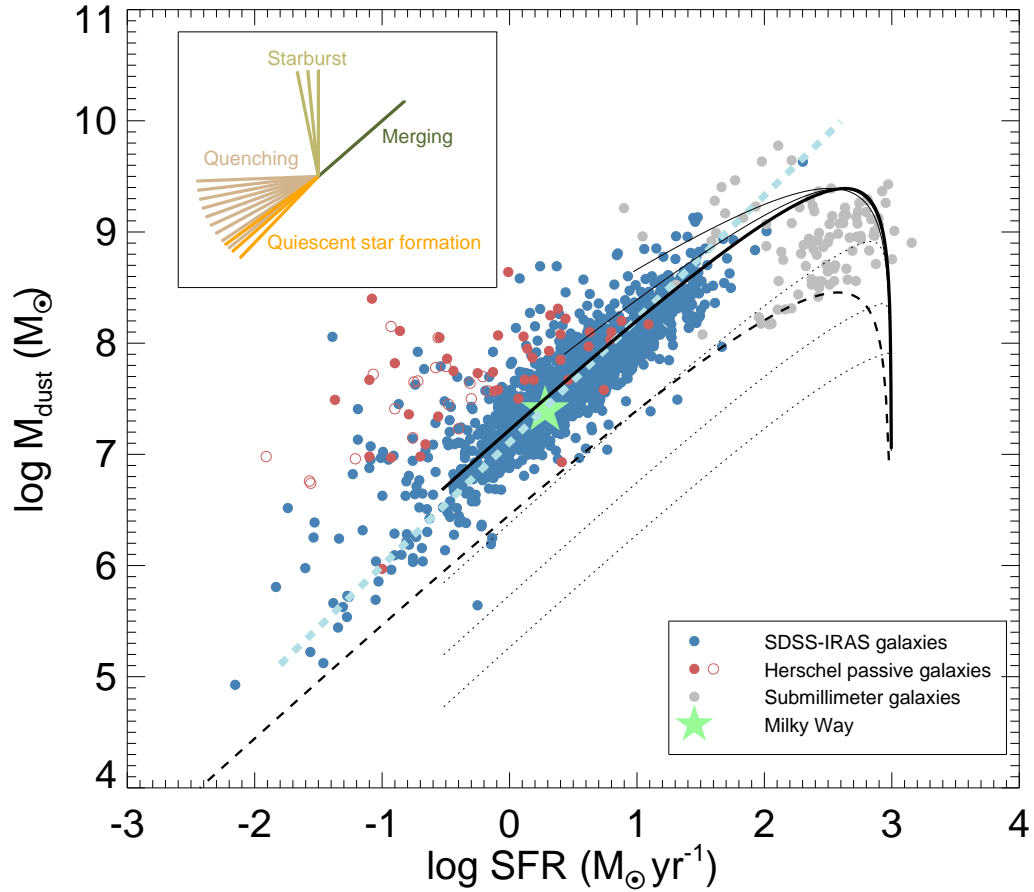


**Figure 1.** The dust mass – star-formation rate relation. Blue symbols: SDSS–IRAS galaxies from da Cunha et al. (2010). Green star: Milky Way (Hjorth et al. 2014). Red symbols: ETGs (filled), passive spirals (open) from Rowlands et al. (2012). Grey symbols: SMGs from Swinbank et al. (2013). The thick dashed pale-blue line is the da Cunha et al. (2010) relation. All SFRs have been computed assuming a Chabrier IMF. Overplotted are models with initial SFRs equivalent to  $1000 M_{\odot} \text{ yr}^{-1}$  for a Chabrier IMF, and gas mass of  $3 \times 10^{11} M_{\odot}$ , as described in Section 3. The thick solid curve is for a bottom-light IMF, no SN dust destruction, and  $k = 0.9$ . Thin solid curves are for  $k = 1$  and  $k = 1.2$ . The thick dashed curve is for a Salpeter IMF. The dotted curves are for  $M_{\text{cl}}$  of 100, 500,  $1500 M_{\odot}$ . The different physical processes shaping the diagram are shown as directions in the upper left corner.